electronics

MDPI

*Article*

# Self-Decoupled MIMO Antenna Realized by Adjusting the Feeding Positions

**Yangyang He [1], Yi-Feng Cheng [1] and Jiang Luo [1,2,*]**

[1] School of Electronics and Information, Hangzhou Dianzi University, Hangzhou 310018, China
[2] State Key Laboratory of Millimeter Waves, Southeast University, Nanjing 210096, China
* Correspondence: luojiang@hdu.edu.cn

**Abstract:** This paper proposes a novel decoupling technique achieved by adjusting the position of feeding probes of antennas. Two inherent radiation modes (patch mode and monopole mode), with different patterns and polarizations, are simultaneously excited by the same feeding probe. High isolation is realized based on manipulating the relationship of two-mode couplings by moving the feeding positions. Since the two radiation modes are generated by the same antenna element, the proposed MIMO antenna features a simple structure and compact size. For verification, a two-element array with center-to-center spacing of 0.404 $\lambda_0$ ($\lambda_0$ is the wavelength in the air) is prototyped and characterized. Simulation and experimental results show that the proposed novel technique can offer higher port isolation (>18.1 dB), increased efficiency (>70%), and a lower envelope correlation coefficient (ECC < 0.1) in the operating frequency band (11.61–12.49 GHz).

**Keywords:** MIMO antenna; mixed radiation modes; decoupling; mutual coupling; self-decoupled antenna

check for updates

**Citation:** He, Y.; Cheng, Y.-F.; Luo, J. Self-Decoupled MIMO Antenna Realized by Adjusting the Feeding Positions. *Electronics* **2022**, *11*, 4004. https://doi.org/10.3390/electronics11234004

Received: 8 November 2022
Accepted: 30 November 2022
Published: 2 December 2022



## 1. Introduction

It is known that the MIMO antenna plays an important role in the 5G communication system due to its high channel capacity, low delay, and outstanding transmission rate [1]. However, the inherent coupling between different radiating elements can decrease the performance of the MIMO system [2]. In recent years, much effort has been put into reducing the mutual couplings between antennas [3–23], including the use of decoupling networks [3,4], electromagnetic band gap (EBG) structure [5], meta-surface [6], defected ground structure (DGS) [7], neutralization line [8], parasitic element [9], and self-decoupled elements [10]. In [11], an inductance-based decoupling structure is presented to decrease the mutual coupling between extremely closely spaced microstrip antennas. A cascaded power dividing decoupling network (C-PDDN) is proposed in [12], and it can reduce the mutual coupling in adjacent or even contiguous frequency bands of the two antennas. The EBG structure is also adopted to enhance the isolation of antenna arrays [13,14]. In [14], a novel slot–array DGS is presented. Additionally, based on the analysis of equivalent circuit model, the DGS can contribute to reducing the mutual coupling with stop-band characteristics. Another well-known decoupling method is by using a neutralization line (NL) [15]. An additional coupling path can be generated by NL to cancel out the original coupling in MIMO antenna arrays [15]. Parasitic elements are used in [16] to decrease the mutual coupling of antennas, and the performance of MIMO system is then enhanced. However, most above-mentioned proposals adopt additional structures (circuit or scatters) for decoupling purpose, which often occupy an excessive volume of space and increase the complexity of the systems. Besides this, the extra structures usually have negative impact on antenna performances, such as reducing the operating bandwidth and decreasing the radiation efficiency. A high isolation air-patch antenna array loaded with vertical resonators was proposed in [17]. However, three-dimensional structure is necessarily required to construct the loaded resonators, which significantly increase the manufacturing complexity. So, the antenna array in [17] cannot be produced (on a large scale) using the traditional printed board technology.

To overcome this problem, a novel and simple self-decoupled design method is proposed in this paper. Two radiation modes create two types of mutual couplings in the patch-monopole antenna array. The feeding position can adjust the strength and phase relationship of two coupling modes. When the two couplings satisfy equal magnitude and out-of-phase relationship, the total coupling can be canceled out, and high isolation is realized. Moreover, the proposed self-decoupled antenna array has the advantages of size miniaturization and simple design, thanks to the elimination of any extra decoupling structure. For demonstration, a compact two-port patch–monopole antenna is designed, fabricated, and characterized. Experimental results reveal that the proposed technique can provide enhanced port isolation (>18.1 dB), increased antenna efficiency (>70%), and improved pattern diversity (ECC < 0.1) in the operating frequency band, with simple and compact construction.

## 2. Proposed Design

Figure 1 shows the structure of the two-port patch–monopole antenna, which is composed of two patch radiators on the top layer of the substrate, a ground plane, and two 50 Ω coaxial feeds. Figure 1b depicts the configuration of the MIMO antenna. The left and right elements are symmetrical about the $x$ axis. The two-port MIMO antenna has a center-to-center spacing of $d$. The single element has a size of $W_C \times L_C$, and the whole PCB size is $W_G \times L_G$. Changing the position of the feed port can adjust the components of patch and monopole modes. High isolation is realized when two-mode couplings are canceled out. Next, a detailed explanation on this decoupling method is illustrated as follows.

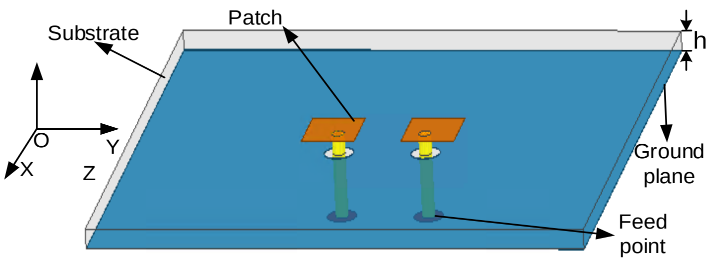


(**a**)

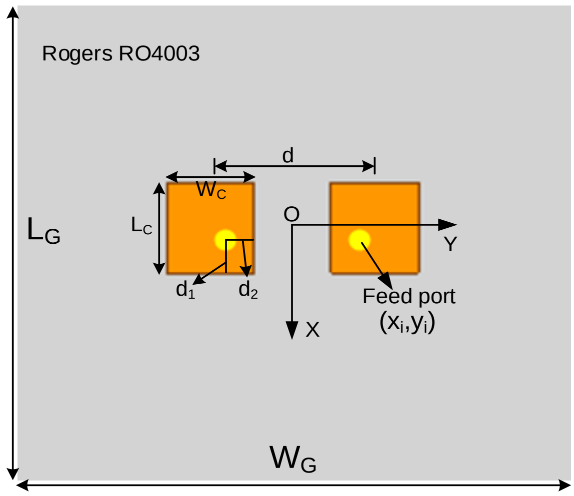


(**b**)

**Figure 1.** Structure of the proposed antenna array. (**a**) Perspective view. (**b**) Top view.

*2.1. A. Radiation Modes and Decoupling Mechanism*

Figure 2 shows two different operating modes of the proposed patch–monopole antenna. For patch mode (Figure 2a), the current flows from one edge of the patch to the other edge. Note that the position of the feeding probe can also change the specific horizontal polarization of the patch mode (for example, the specific polarization could be along the $x$-direction, $y$-direction, or other directions). For the monopole mode (Figure 2b), the current starts from the end of feeding probe (near the ground), flowing upwards, and then going to the edges of the patch. In principle, these two modes co-exist (more or less) for every feeding position. However, their strength and phase relationships are quite different (for different positions). For better demonstration, as shown in Figure 1b, the center of the dielectric substrate is defined as the coordinate origin (O). Therefore, the location (taking right element as reference) of the feed port can be represented by coordinate points ($X_i$, $Y_i$). The solid line in Figure 3 shows two special cases (unit: mm) when the patch mode and monopole mode are dominated, respectively. The middle pattern between two specific radiation modes is shown by the dotted line in Figure 3. At location (1.275, 5), the feeding probe is in the middle line of the patch (similar to the feeding approach of a traditional patch). The patch mode is then dominated, which resulted in broadside radiation. However, at location (0, 5), the feeding probe is at the center of the patch. Since the center position is a virtual-ground (0 voltage) condition for patch mode, this position can only excite monopole mode, which resulted in end-fire radiation. It is worth mentioning that, by adjusting the position of the feed point $X_i$ from 0 to 0.125, it can be observed that the radiation mode is similar to the monopole mode, but there is already a trend of broadside radiation. Continuing to adjust $X_i$ from 0.125 to 0.425, broadside radiation is further increased. The simulated results illustrate the existence of two radiation modes of the proposed patch–monopole antenna, and some intermediate modes can be obtained by adjusting the feed point position $X_i$.

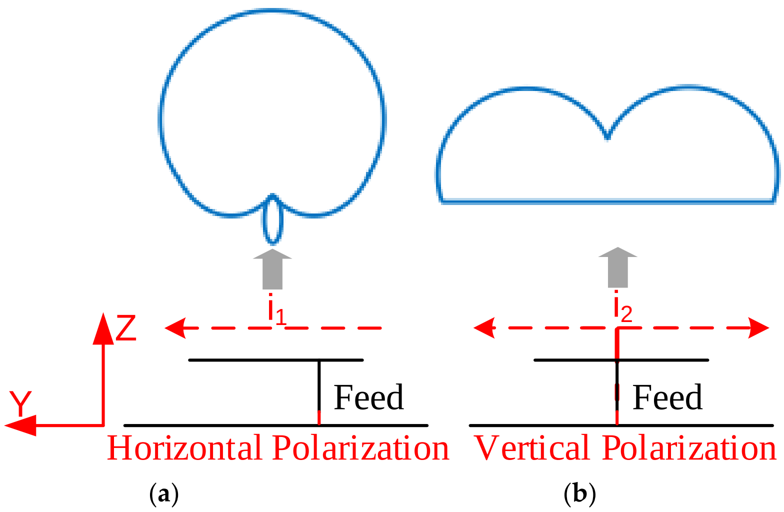


**Figure 2.** Radiation modes. (**a**) Patch mode. (**b**) Monopole mode.

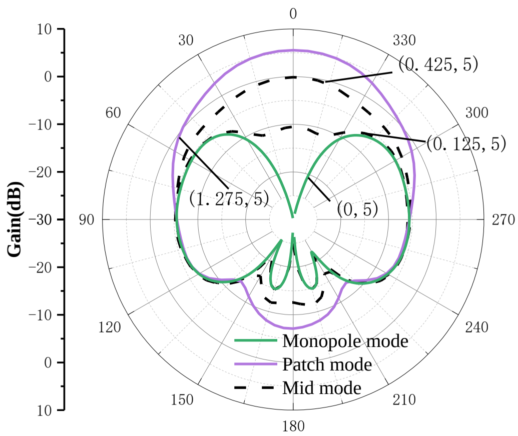


**Figure 3.** Radiation modes (at 12.12 GHz) of proposed antenna with different feeding positions. Unit: mm.

Obviously, since there are two radiation modes for every antenna, two types of mutual couplings co-exist in the proposed array. The relative strengths and phases of the two radiation modes are controlled by tuning the coordinate point of the feed probe. Correspondingly, the coupling paths are also modified when modifying the feeding position. It can be concluded that, if the amplitudes of two coupling paths are equal, and their phases are opposite, the mutual coupling can be totally cancelled out, and high port isolation is then achieved. The freedom of feeding position is mainly used for decoupling purposes. As for the impedance matching of antennas, it is simply realized by adjusting the width ($W_C$) of the patch.

## 2.2. B. Simulation Verification

To further verify the decoupling mechanism of the proposed technique, the patch–monopole antenna arrays with different feeding points are simulated by using an EM simulator. The antennas are fed by 50 Ω coaxial lines from the back of the ground. The center-to-center distance between two patches is 0.404 $\lambda_0$, where $\lambda_0$ is the wavelength in free space. Figure 4 shows the simulated scattering parameters of the patch–monopole antenna with different feeding positions. It is obvious that, in the frequency band (11.65–12.58 GHz) with return loss under −10 dB, the mutual coupling is reduced step by step with the altering of coordinate positions. Moreover, the port isolation is enhanced by about 3.5 dB~24.09 dB in the operating band.

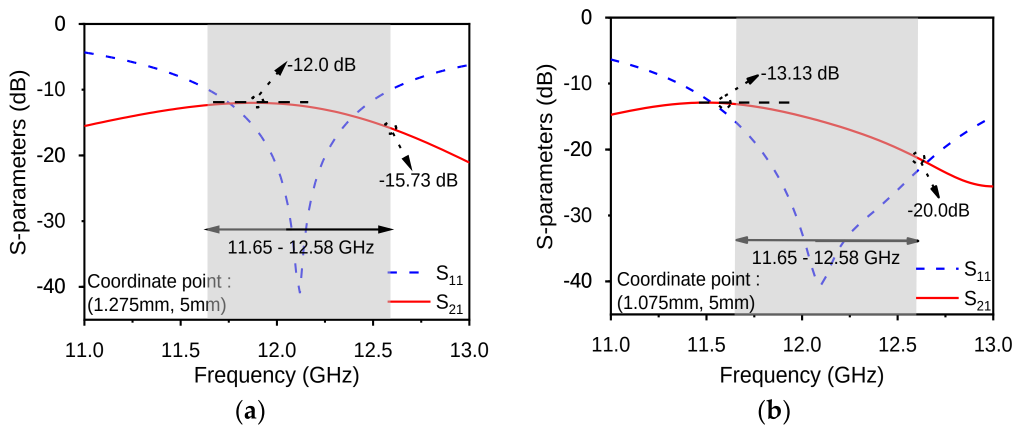


**Figure 4.** *Cont.*

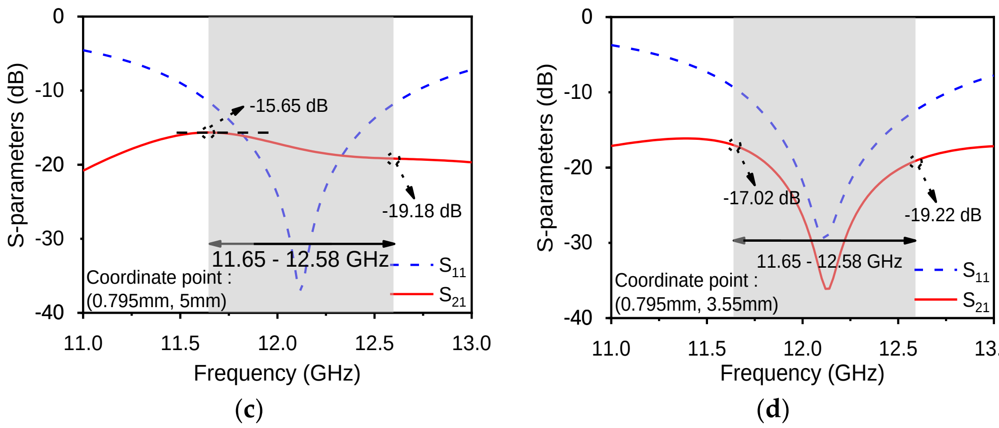


**Figure 4.** Simulated S−parameters of path−monopole antenna array with different coordinate points of feed probe. (**a**) (1.275 mm, 5 mm); (**b**) (1.075 mm, 5 mm); (**c**) (0.795 mm, 5 mm); and (**d**) (0.795 mm, 3.55 mm).

Figure 5 gives the electric filed distribution for the reference and proposed antenna arrays. The feeding position of coupled antenna for the reference array exhibits high electric filed. The feeding position of the coupled antenna for the proposed array shows a null-filed-position (equivalent to short-circuited condition). Therefore, the isolation is enhanced after decoupling.

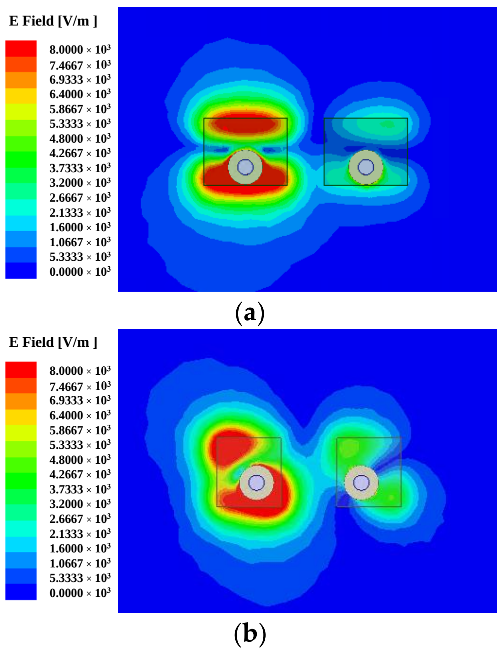


**Figure 5.** Electric filed distribution for the reference and proposed antenna arrays. (**a**) Reference. (**b**) Proposed.

## 3. Experimental Validation

The proposed antenna array with center-to-center spacing of 0.404 $\lambda_0$ is designed, fabricated, and measured. A reference array based on traditional patch antennas is also designed and characterized for comparison. Rogers RO4003 is selected to fabricate the dielectric substrate, whose dielectric constant is 3.55, loss tangent is 0.0027, and thickness is 1.542 mm. The photographs of fabricated MIMO antennas are depicted in Figure 6, and the dimensions of antennas are shown in Table 1. The S-parameters of MIMO antennas are recorded by the Vector Network Analyzer (VNA), with frequency ranging from 11 to

13 GHz. Figure 7 shows the measured S-parameters of both arrays. It can be seen that the frequency band with reflection coefficient under −10 dB is from 11.61 to 12.49 GHz, and the port-isolation of the proposed antenna is improved by about 6~32 dB in comparison to the reference one. It is observed that the proposed MIMO antenna has a smaller frequency deviation than the reference one. The difference is mainly due to the manufacturing errors of substrate, welding, and test environment. The total efficiency and radiation patterns are measured by a microwave chamber (Figure 6e). When one antenna port is excited for measurement, another port is terminated by a 50 Ω load. Figure 8 shows the measured efficiency of two antenna arrays. Obviously, in the operating band, more than 10% of the total efficiency is increased after using the proposed decoupling method. Figure 9 gives the measured ECC values (far-field) of both arrays. The proposed patch–monopole array has much lower ECC (<0.1) than the traditional patch array (>0.5). Figure 10 shows the radiation patterns of the arrays. In summary, the performance of the proposed array is much better than the reference array.

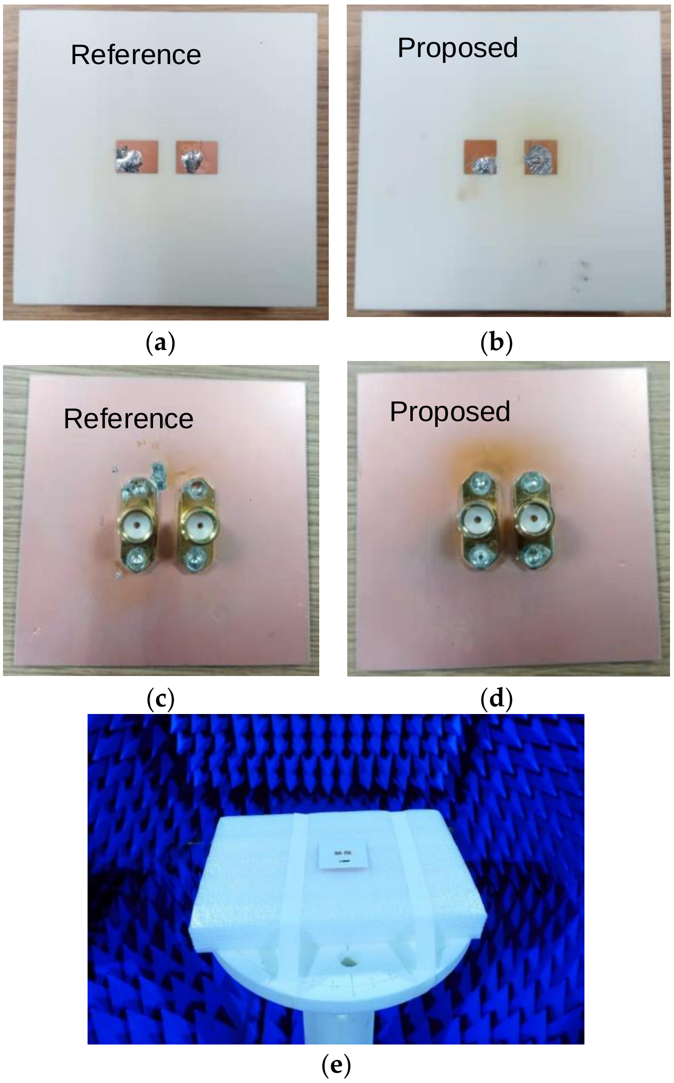


**Figure 6.** Photographs of fabricated arrays. (**a**,**b**): Front view. (**c**,**d**): Back view. (**e**) Measurement setup in an antenna chamber.

**Table 1.** Dimensions of fabricated antennas. (Unit: mm).

| | $L_G$ | $W_G$ | d | $L_C$ | $W_C$ | $d_1$ | $d_2$ |
|---|---|---|---|---|---|---|---|
| Reference | 50 | 50 | 10 | 5.555 | 6.9 | 1.5 | 4.5 |
| Proposed | 50 | 50 | 10 | 5.700 | 5.3 | 1.98 | 2.0 |

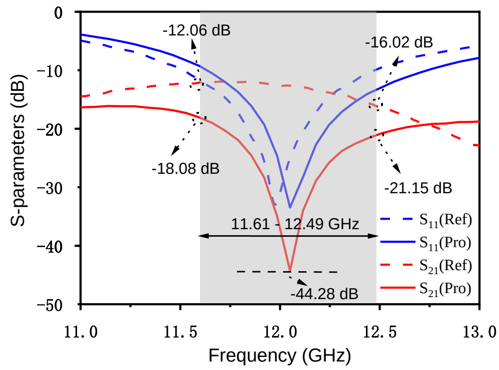


**Figure 7.** Measured S−parameters of reference and proposed design.

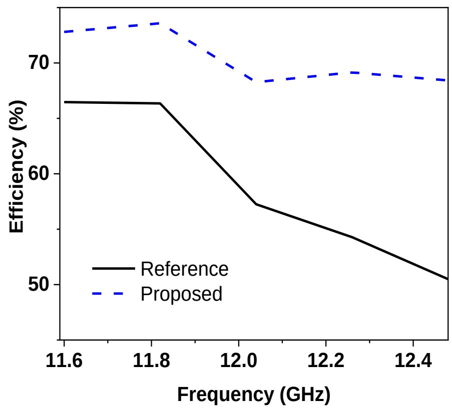


**Figure 8.** Measured total efficiency.

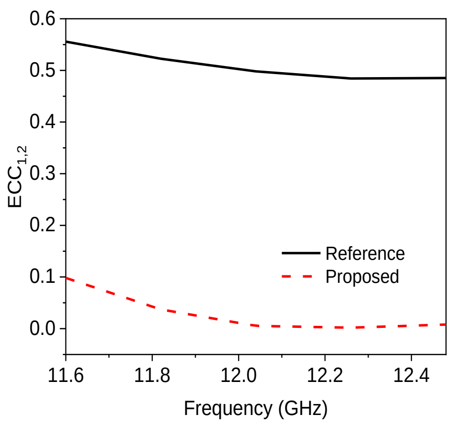


**Figure 9.** ECC values (calculated from far-field data).

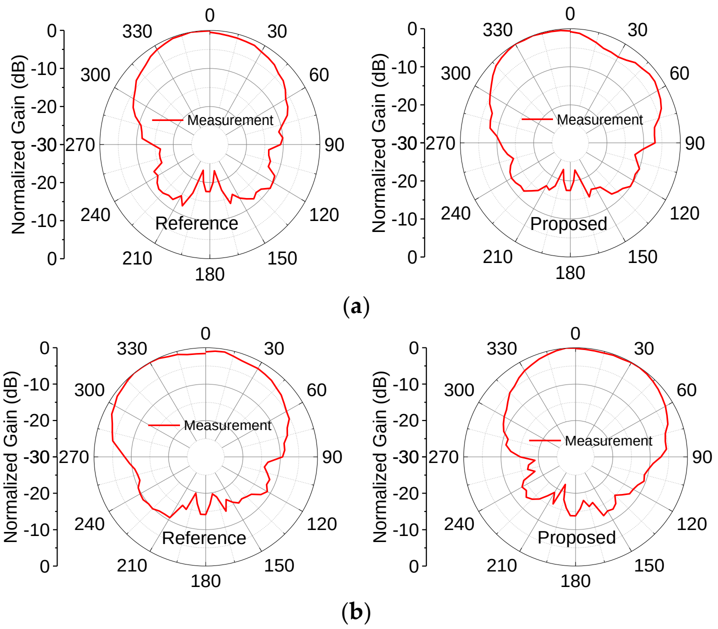


**Figure 10.** Measured radiation patterns at center frequency. (**a**) *xoz*−plane. (**b**) *yoz*−plane.

Table 2 shows the comparison of the proposed antenna with recently published designs. The performance of the proposed antenna is competitive compared to other antenna designs. In addition, this method requires no additional decoupling structure, which makes the design simple and compact.

**Table 2.** Comparison with other decoupling methods.

| Ref. No. (Year) | Additional Structure | Element Spacing | Frequency (GHz) | Isolation Enhancement | Peak Efficiency |
|---|---|---|---|---|---|
| [11] (2020) | Required (Connect-Strip) | 0.440 $\lambda_0$ | 2.39–2.53 | 10 dB | 87% |
| [14] (2020) | Required (DGS) | 0.504 $\lambda_0$ | 1.25–1.27 | 5 dB/15 dB | N.A. |
| [18] (2019) | Required (Resonators) | 0.260 $\lambda_0$ | 2.20–2.23 | 12 dB | 74% |
| [19] (2020) | Required (Natura Line) | N.A. | 0.94–0.99 | 17 dB | N.A. |
| This work | Not Required | 0.404 $\lambda_0$ | 11.61–12.49 | 7 dB | 73% |

## 4. Conclusions

This paper proposes a novel decoupling technique to improve the port isolation of two-port MIMO antennas. In traditional patch arrays, there exist strong mutual couplings between two antenna elements. However, by adjusting the position of feeding probes, two types of mutual couplings are canceled out, and high isolation is then realized. The proposed MIMO antenna has huge superiority thanks to its compact structure, smaller size, and easier manufacturing. The proposed patch–monopole MIMO antenna is a good candidate for modern wireless communication systems.

**Author Contributions:** Conceptualization, Y.H. and J.L.; Methodology, Y.H.; Writing—original draft, Y.H.; Data curation, Y.-F.C.; Formal analysis, Y.-F.C.; Writing—review and editing, Y.-F.C.; Supervision, J.L.; Project administration, J.L. All authors have read and agreed to the published version of the manuscript.

**Funding:** This research was supported in part by the Fundamental Research Funds for the Provincial Universities of Zhejiang under Grant GK229909299001-016 and GK229909299001-309, in part the

State Key Laboratory of Millimeter Waves, Southeast University under Grant K202316, and in part by the National Natural Science Foundation of China under Grant 62201183.

**Data Availability Statement:** The data presented in this work are available within the article.

**Conflicts of Interest:** The authors declare no conflict of interest.

## References

1. Jensen, M.A.; Wallace, J.W. A review of antennas and propagation for MIMO wireless communications. *IEEE Trans. Antennas Propag.* **2004**, *52*, 2810–2824. [CrossRef]
2. Wallace, J.; Jensen, M. Mutual coupling in MIMO wireless systems: A rigorous network theory analysis. *IEEE Trans. Wirel. Commun.* **2004**, *3*, 1317–1325. [CrossRef]
3. Li, M.; Jiang, L.; Yeung, K.L. Novel and efficient parasitic decoupling network for closely coupled antennas. *IEEE Trans. Antennas Propag.* **2019**, *67*, 3574–3585. [CrossRef]
4. Xia, R.L.; Qu, S.W.; Li, P.F.; Jiang, Q.; Nie, Z.P. An efficient decoupling feeding network for microstrip antenna array. *IEEE Antennas Wirel. Propag. Lett.* **2015**, *14*, 871–874. [CrossRef]
5. Farahani, H.S.; Veysi, M.; Kamyab, M.; Tadjalli, A. Mutual coupling reduction in patch antenna arrays using a UC-EBG superstrate. *IEEE Antennas Wirel. Propag. Lett.* **2010**, *9*, 57–59. [CrossRef]
6. Iglesias, E.R.; Teruel, O.Q.; Sanchez, L.I. Planar soft surface and their application to mutual coupling reduction. *IEEE Trans. Antennas Propag.* **2009**, *57*, 3852–3859. [CrossRef]
7. Ghosh, J.; Mitra, D.; Das, S. Mutual coupling reduction of slot antenna array by controlling surface wave propagation. *IEEE Trans. Antennas Propag.* **2019**, *67*, 1352–1357. [CrossRef]
8. Wang, Y.; Du, Z. A wideband printed dual-antenna with three neutralization lines for mobile terminals. *IEEE Trans. Antennas Propag.* **2014**, *62*, 1495–1500. [CrossRef]
9. Chen, X.M.; Tang, M.C.; Yi, D.; Ziolkowski, R.W. Wideband, compact antennas with interdigitated magnetic-based near-field resonant parasitic elements. *IEEE Trans. Antennas Propag.* **2021**, *69*, 5036–5041. [CrossRef]
10. Lin, H.W.; Chen, Q.G.; Ji, Y.; Yang, X.J.; Wang, J.P.; Ge, L. Weak-field-based self-decoupling patch antennas. *IEEE Trans. Antennas Propag.* **2020**, *68*, 4208–4217. [CrossRef]
11. Sun, L.B.; Li, Y.; Zhang, Z.J. Decoupling between extremely closely spaced patch antennas by mode cancellation method. *IEEE Trans. Antennas Propag.* **2021**, *69*, 3074–3083. [CrossRef]
12. Li, M.; Wang, M.; Jiang, L.J.; Yeung, L.K. Decoupling of antennas with adjacent frequency bands using cascaded decoupling network. *IEEE Trans. Antenna Propag.* **2021**, *69*, 1173–1178. [CrossRef]
13. Jeong, J.W.; Park, J.S. A microcontroller unit-based electromagnetic bandgap control scheme: Application for enhancing isolation in an antenna array and the EMI scanner system speed thereof. *IEEE Trans. Microw. Theory Tech.* **2020**, *68*, 4536–4553. [CrossRef]
14. Gao, D.; Cao, Z.X.; Fu, S.D.; Quan, X.; Chen, P. A novel slot-array defected ground structure for decoupling microstrip antenna array. *IEEE Trans. Antennas Propag.* **2020**, *68*, 7027–7038. [CrossRef]
15. Li, M.; Jiang, L.J.; Yeung, K.L. A general and systematic method to design neutralization lines for isolation enhancement in MIMO antenna arrays. *IEEE Trans. Veh. Technol.* **2020**, *69*, 6242–6253. [CrossRef]
16. Li, Z.Y.; Du, Z.W.; Takahashi, M.; Saito, K.; Ito, K. Reducing mutual coupling of MIMO antennas with parasitic elements for mobile terminals. *IEEE Trans. Antennas Propag.* **2012**, *60*, 473–481. [CrossRef]
17. Cheng, Y.-F.; Cheng, K.-K.M. Decoupling of 2 × 2 MIMO Antenna by Using Mixed Radiation Modes and Novel Patch Element Design. *IEEE Trans Antennas Propag.* **2021**, *69*, 8204–8213. [CrossRef]
18. Li, M.; Zhong, B.G.; Cheung, S.W. Isolation enhancement for MIMO patch antennas using near-field resonators as coupling-mode transducers. *IEEE Trans. Antennas Propag.* **2019**, *67*, 755–764. [CrossRef]
19. Cheng, Y.F.; He, Y.; Wu, W.; Chen, C.; Wang, G. Wideband decoupling technique for two-element antenna array by using pixel neutralization line. *Microw. Opt. Technol. Lett.* **2022**, *64*, 1785–1792. [CrossRef]
20. Abbas, A.; Hussain, N.; Sufian, M.A.; Jung, J.; Park, S.M.; Kim, N. Isolation and Gain Improvement of a Rectangular Notch UWB-MIMO Antenna. *Sensors* **2022**, *22*, 1460. [CrossRef]
21. Sufian, M.A.; Hussain, N.; Abbas, A.; Lee, J.; Park, S.G.; Kim, N. Mutual Coupling Reduction of a Circularly Polarized MIMO Antenna Using Parasitic Elements and DGS for V2X Communications. *IEEE Access* **2022**, *10*, 56388–56400. [CrossRef]
22. Bayarzaya, B.; Hussain, N.; Awan, W.A.; Sufian, M.A.; Abbas, A.; Choi, D.; Lee, J.; Kim, N. A Compact MIMO Antenna with Improved Isolation for ISM, Sub-6 GHz, and WLAN Application. *Micromachines* **2022**, *13*, 1355. [CrossRef] [PubMed]
23. Roshani, S.; Shahveisi, H. Mutual Coupling Reduction in Microstrip Patch Antenna Arrays Using Simple Microstrip Resonator. *Wirel. Pers. Commun.* **2022**, *126*, 1665–1677. [CrossRef]